THE JOURNAL OF PHYSICAL CHEMISTRY B

Article

pubs.acs.org/JPCB

Dynamics of Glass Forming Ammonia Hydrates

H. Didzoleit,[†] M. Storek,[†] C. Gainaru,[†] B. Geil,[‡] and R. Böhmer*[,†]

[†]Fakultät für Physik, Technische Universität Dortmund, 44221 Dortmund, Germany

[‡]Institut für Physikalische Chemie, Georg-August-University Göttingen, 37077 Göttingen, Germany

ABSTRACT: The dielectric relaxation of ammonia−water mixtures was studied for a range of NH_3 mole fractions x. For $0.01 \leq x < 0.33$, the samples can be supercooled relatively easily. In this composition range, the relaxation strength is proportional to x. The dielectric relaxation times display a super-Arrhenius behavior, are independent of the NH_3 content in the specified range, and, for $T > 250$ K, line up smoothly with those of pure water. The relaxation behavior of glass forming ammonia hydrates was also investigated using nuclear magnetic resonance techniques including deuteron relaxometry and stimulated-echo spectroscopy, as well as static field-gradient proton diffusometry. These experiments yielded additional insights into the rotational and translational dynamics of ammonia hydrates.

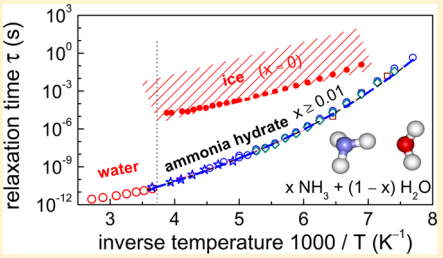

I. INTRODUCTION

Ammonia containing ices and hydrates are relevant for several satellites in the outer solar system.[1] Laboratory studies have shown that water−ammonia mixtures form a rich variety of solid phases including the stoichiometric compounds ammonia di-, mono-, and hemihydrate. These crystalline ammonia hydrates were studied using diffraction and calorimetry as well as by infrared and dielectric spectroscopy.[2−10] The composition−temperature phase diagram[11−13] of $(H_2O)_{1-x}(NH_3)_x$ shows that H_2O and ammonia monohydrate, $H_2O{\cdot}NH_3$, form a deep eutectic near the composition of ammonia dihydrate. Close to the eutectic point with x near 0.37 and temperatures near 175.4 K, a peritectic point exists with $x \approx 0.35$ and $T \approx 176.2$ K. The water rich part of the phase diagram ($x < 0.3$) is of particular interest in the planetary sciences, although often additional ingredients such as, e.g., sulfates are relevant[14,15] and pressure effects play an important role.[16,17] Ammonia is a significant constituent (with NH_3 mole fractions probably up to about 15%)[13] on some icy moons in the outer solar system, and the corresponding mixtures were suggested to act as cryovolcanic lava on these cold satellites.[18−20]

The complexities of the phase diagram can render the establishment of phase equilibria difficult in certain composition ranges, and it is not surprising that glass formation has been reported to occur.[21] Glass transition temperatures of about 120 K[22] and 128 K[21] were variously reported and found to be independent of composition up to the eutectic mole fraction. Often used as an antifreeze agent, NH_3 is known to inhibit crystallization not only near the deep eutectic at which the aqueous ammonia solution can be quite viscous but also at lower concentrations.

The structural and vibrational properties of many of the crystalline ammonia hydrate phases were intensively investigated, but the dynamics in the supercooled liquid regime has attracted much less attention. Although some calorimetry[21,22] and viscosity[23] data are available, little is known about the local dynamics of viscous ammonia hydrate liquids. Therefore, we carried out dielectric and nuclear magnetic resonance (NMR) experiments on $(H_2O)_{1-x}(NH_3)_x$ samples for $0.01 \leq x < 0.33$, which can be supercooled easily. We have also performed dielectric measurements for NH_3 mole fractions lower than approximately 1% and found that in this concentration range crystallization always occurred.

II. SAMPLES AND EXPERIMENTS

All ammonia hydrate samples, except the ones used for ^2H NMR, were prepared from liquid mixtures obtained by weighing appropriate quantities of a 25 wt % NH_3 aqueous solution, i.e., ∼26.07 mol % (Merck, stated purity 99.7%), with bidestilled water. For a partially deuterated ammonia hydrate sample with $x = 0.1$ that was used for ^2H NMR experiments, the protonated NH_3 aqueous solution was mixed with D_2O (Sigma Aldrich, stated purity 99.99%) and was then flame-sealed in a glass tube.[24] The resulting D/H ratio thus was about 1.3. A sample with composition $(D_2O)_{0.67}(NH_3)_{0.33}$ (i.e., D/H ratio of 1.33) was produced by condensing pure ammonia gas (from Linde Co., stated purity 99.98%) at temperatures <170 K. Afterward the D_2O ice was added. Then, the mixture was heated to just above the melting point and stirred. The sample was subsequently quenched to liquid nitrogen temperatures at which it was ground under dry conditions with mortar and pestle and filled into a precooled glass tube, which was then flame-sealed. During this procedure and the subsequent transfer to the NMR cryostat, care was taken that temperatures of ∼100 K were not exceeded. Deuteron NMR was performed at a Larmor frequency of $\omega_L = 2\pi \times 46.46$ MHz. For the acquisition

Received: July 30, 2013
Revised: September 9, 2013
Published: September 10, 2013

of spin-relaxation and stimulated-echo data standard procedures were employed.[25]

For the dielectric experiments, the solutions were pipetted into a Hastelloy/sapphire cell designed as described previously.[26] Prior to the measurements, the cell was usually cooled down to 200 K with an average rate of 3 K/min. During data acquisition, the temperature was stabilized within 0.1 K using a Quatro controller. Spectra recorded during cooling and reheating were practically identical, indicating that no unintended crystallization occurred during the investigation. The dielectric experiments were performed using an Alpha analyzer from Novocontrol covering the frequency range 0.1 Hz $\leq \nu \leq$ 1 MHz. For a sample with x = 0.1, additional measurements were recorded up to 1 GHz.

III. RESULTS AND ANALYSES

A. Dielectric Spectroscopy. As examples of the experimental results obtained for various ammonia concentrations, in Figure 1a–d we show frequency spectra of the complex dielectric constant, $\varepsilon^*(\nu) = \varepsilon'(\nu) - i\varepsilon''(\nu)$, for NH_3 doping levels of x = 0.01 (frames a and b) and 0.26 (frames c and d). Real and imaginary parts of ε^* reveal the existence of a dielectric relaxation process as well as of significant electrical dc conductivity σ_0. The latter can be regarded as the low-frequency limit of $\sigma^*(\nu) = i2\pi\nu\varepsilon_0\varepsilon^*(\nu)$ with ε_0 designating the permittivity of free space. Overall, the results for the two concentrations look very similar, only the loss peak amplitudes and the relaxation strengths $\Delta\varepsilon$ differ considerably.

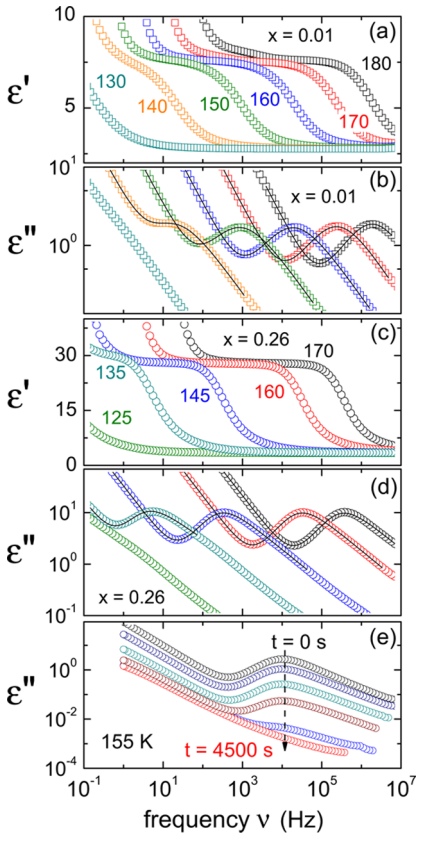

Figure 1. (a) Dielectric constant and (b) dielectric loss of a supercooled ammonia hydrate with x = 0.01. Frames c and d are the same for x = 0.26. The lines are fits using eq 1. The numbers in frames a–d are temperatures in Kelvin. Frame e shows data recorded during the crystallization of $(H_2O)_{0.75}(NH_3)_{0.25}$ at 155 K. From top to bottom, the acquisition of the spectra started at t = 0, 330, 670, 1250, 1800, and 4500 s after the base temperature was reached. The acquisition of each spectrum took about 165 s.

In order to extract $\Delta\varepsilon$ as well as dielectric relaxation times τ quantitatively, we used the Cole–Davidson equation[27] to which a term was added that accounts for a conductivity contribution so that overall one has

$$\varepsilon^*(\nu) = \varepsilon_\infty + \frac{\Delta\varepsilon}{(1 + 2\pi i\nu\tau)^{\gamma_\varepsilon}} + \frac{\sigma_0}{2\pi i\varepsilon_0\nu} \quad (1)$$

Here, ε_∞ denotes the high-frequency dielectric constant and the parameter γ_ε is a measure for the width of the distribution of relaxation times. The results in Figure 1a–d show that eq 1 provides excellent fits. We find that the width parameter is γ_ε = 0.65 ± 0.05 for all x and T and that the relaxation strengths turned out to be independent of temperature. The concentration dependence of $\Delta\varepsilon$ is presented in Figure 2 and one recognizes an overall linear trend, $\Delta\varepsilon \propto x$, for x > 0.01. The implication of these results will be discussed in section IV. There, we will also present the temperature dependence of the relaxation times, which, as we find, do not depend on the ammonia concentration.

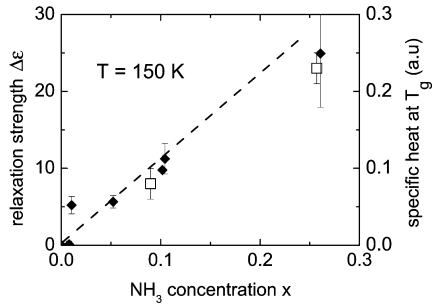

Figure 2. Concentration dependence of the dielectric relaxation strength (filled diamonds, this work) and specific heat step near T_g (open squares, ref 22) for supercooled ammonia hydrates. The dashed line marks a linear concentration dependence.

In order to check that the samples with x > 0.01 are in fact supercooled liquids, we kept them at suitable constant temperatures for extended periods of time. As an example, in Figure 1e, we show loss spectra for $(H_2O)_{0.75}(NH_3)_{0.25}$ recorded at T = 155 K after the sample was initially cooled from room temperature to 100 K with an average rate of 10 K/min and then heated with the same rate to 155 K. Figure 1e clearly reveals that the relaxation peak vanishes completely within a period of ~75 min, thus demonstrating that initially the material was in an amorphous state. The time that is required for crystallization is compatible with that from previous calorimetric data.[22]

For a quantitative analysis of the crystallization data shown in Figure 1e we used $\varepsilon''(t) \propto \exp\{-[(t - t_0)/\tau_x]^{AE}\}$,[28] an expression known as the Johnson–Mehl–Avrami–Kolmogorov (JAMK) equation. After the base temperature is reached, crystal growth is typically initiated after some induction period t_0, which we use as a fitting parameter. The interplay of nucleation and crystal growth leads to an effective time constant τ_x. The Avrami exponent AE in the JAMK equation depends on the dimensionality of the growth process[29] and varies typically between 1 and 4. For the measurements shown in Figure 1e, we obtain τ_x = (800 ± 100) s and AE = 1.15 ± 0.20. An exponent

dx.doi.org/10.1021/jp407581q | J. Phys. Chem. B 2013, 117, 12157–12163

close to unity indicates that the crystallization mechanism may be governed by one-dimensional growth of preexisting nuclei.[29]

B. NMR Spectroscopy. In order to probe the translational and rotational dynamics in the ammonia hydrates further, we performed various proton and deuteron NMR experiments. Using ^{2}H NMR we exploited that the quadrupolarly perturbed frequency

$$\omega_Q = \pm\frac{1}{2}\delta_Q(3\cos^2\theta - 1 - \eta\sin^2\theta\cos 2\phi) \quad (2)$$

of the deuteron in an N−D or C−D bond depends on the polar angle θ that such a bond encloses with the external magnetic field. The azimuthal angle ϕ is defined as usual. Furthermore, δ_Q denotes the effective anisotropy parameter which is a measure of the quadrupolar coupling constant.[30,31] To probe the molecular motion directly, stimulated-echo spectroscopy was performed and yielded the ensemble averaged ($\langle\ldots\rangle$) two-time correlation function

$$F_2(t_p, t_m) = \langle\cos[\omega_Q(0)t_p]\cos[\omega_Q(t_m)t_p]\rangle, \quad (3)$$

which depends on the mixing time t_m and on the evolution time t_p. As an experimentally adjustable parameter, the latter allows one to set the geometrical sensitivity of the experiment. In brief, the decay time τ_2 of F_2 is insensitive to t_p if the jump angles φ of the bond orientations are large, and τ_2 decreases more and more with increasing t_p if φ becomes smaller and smaller.[32]

In Figure 3a we compile representative deuteron stimulated-echo amplitudes $F_2(t_m)$ for x = 0.33 recorded at 133 K for a range of evolution times. The data were fitted using a stretched exponential function, $\propto \exp[-(t_m/\tau_2)^\beta]$, with τ_2 and β denoting motional correlation time and Kohlrausch exponent, respectively. As one can see in Figure 3a, the fits are excellent. The resulting fitting parameters are $\tau_2 = (6 \pm 2)$ ms and $\beta = 0.40 \pm 0.06$, both independent of t_p within experimental error. The finding of an approximately constant $\tau_2(t_p)$ demonstrates that a large-angle jump motion governs the reorientation process. The correlation times τ_2 obtained at 133 K and at slightly different temperatures are added to Figure 5 and are seen to agree reasonably well with the dielectric data.

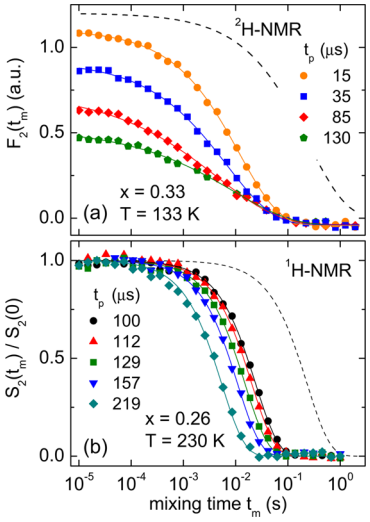

Figure 3. Stimulated-echo curves for supercooled ammonia hydrate liquids. (a) Deuteron data for x = 0.33 recorded in a homogeneous magnetic field at T = 133 K in order to determine rotational correlation times. The solid lines are fits using the stretched exponential function, given in section III.B. (b) Proton stimulated echoes were recorded for x = 0.26 in a magnetic field gradient at T = 230 K in order to determine translational diffusion coefficients using eq 5. In both frames, the dashed lines indicate an appropriately scaled longitudinal magnetization decay.

Furthermore, we measured the recovery of the longitudinal deuteron magnetization $M(t)$ subsequent to pulse perturbation. The magnetization was fitted using $M(t) \propto \exp[-(t/T_1)^\mu]$. Here, T_1 is the spin−lattice relaxation time, and μ is an exponent that parametrizes the deviations from exponential behavior. Results for samples with x = 0.1 and 0.33 are shown in Figure 4. For x = 0.33, data from three different runs on quenched glassy and supercooled liquid samples are shown. Somewhat below the eutectic temperature the samples exhibit a stronger tendency to crystallize. Therefore between about 135 and 160 K no data are reported for the x = 0.33 sample, see Figure 4. The data below this temperature were obtained in a first run on a quenched sample. For x = 0.33, a T_1 minimum was detected near 203 K, showing that below this temperature the molecular dynamics is slow on the time scale, $1/\omega_L \approx 2$ ns, set by the Larmor frequency. From Figure 4 it appears that the data from one of the runs are slightly shifted by about 2−3 K with respect to the others. Overall, however, reasonable agreement is noted when comparing the results from the different runs.

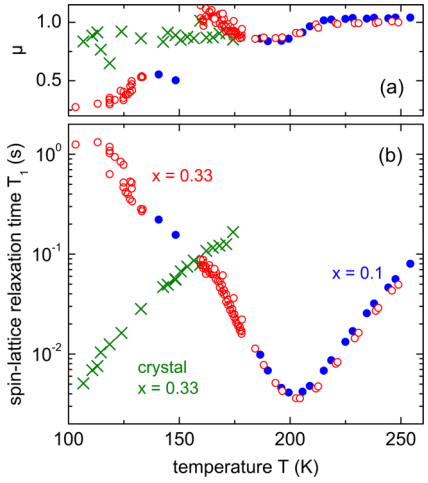

Figure 4. Temperature dependence of (a) the stretching parameter μ chracterizing the magnetization curves and (b) the spin−lattice relaxation times T_1 for samples with x = 0.1 and 0.33. The figure indicates that the μ and T_1 values characterizing the glass forming liquid with x = 0.33 differ widely from those of the crystalline phase (of the same composition).

Spin−lattice relaxation times for a *crystallized* x = 0.33 sample were also measured for T < 180 K, i.e., below the eutectic temperature. Now a completely different temperature dependence is evident, which indicates that in the crystal, motion on a time scale faster than 2 ns prevails in the temperature range covered in Figure 4. Crystallization is easily recognized from the $M(t)$ curves or the resulting spin−lattice relaxation times except for temperatures near 160 K, at which the T_1 times of both phases are very similar.

Furthermore, a sample with x = 0.1 was measured in a T range from about 150 to 250 K and a T_1 minimum was detected near 200 K. Toward lower temperatures the data connect smoothly with those for x = 0.33 indicating that the

dx.doi.org/10.1021/jp407581q | J. Phys. Chem. B 2013, 117, 12157−12163

dynamics in the glass forming samples is practically independent of the composition.

All $M(t)$ data were fitted using a Kohlrausch function, and the stretching coefficients μ for the various samples are shown in Figure 4a. For x = 0.1 and 0.33, one recognizes that upon cooling nonexponential magnetization recovery commences to occur already at temperatures near the T_1 minimum. This finding is to be related with the presence of deuterons in two different (i.e., in O-D and N-D) chemical bonds and correspondingly of different quadrupolar coupling constants. This also leads to bimodal solid-echo spectra that were acquired at temperatures near and below 150 K (not shown). Via fits using $M(t) \propto \exp[-(t/T_1)^{\mu}]$, this bimodality is mapped onto relatively small stretching coefficients μ, seen in Figure 4a for T < 150 K. Near 160 K these coefficients are anomalously large suggesting again that partial crystallization could be affecting the results. For the fully crystallized sample of the ammonia dihydrate composition, however, an almost exponential magnetization recovery is mostly found, consistent with a fast, ergodicity preserving dynamics present in the crystal.

For a quantitative analysis of the spin–lattice relaxation times, the data taken in the range 180 K < T < 260 K, i.e., sufficiently close to the T_1 minimum, are most suitable. Our analysis is based on the classical Bloembergen, Purcell, and Pound (BPP)[33] expression

$$\frac{1}{T_1} = \frac{2\tilde{\delta}_Q^{\,2}}{15}[J(\omega_L) + 4J(2\omega_L)]. \tag{4}$$

Here $\tilde{\delta}_Q$ denotes the fluctuating part of the effective quadrupolar coupling constant and $J(\omega)$ is the spectral density. Like above, we assumed a Cole–Davidson distribution of correlation times leading to $J(\omega_L) = \omega_L^{-1}(1 + \omega_L^{\,2}\tau^2)^{-\gamma/2} \sin[\gamma \arctan(\omega_L\tau)]$. Here $\gamma \leq 1$ measures the distribution width with γ = 1 corresponding to single-exponential relaxation. Using $\omega_L = 2\pi \times 46.2$ MHz, $\tilde{\delta}_Q = 2\pi \times 107$ kHz, and γ = 0.65, we obtained the motional correlation times depicted in Figure 5.

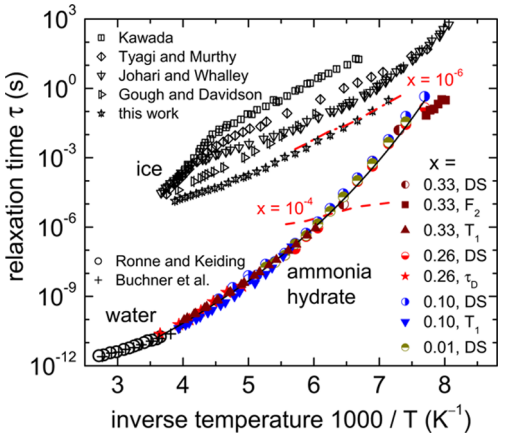

Figure 5. Arrhenius plot of the time constants of glass forming ammonia hydrate liquids, covering the mole fraction range 0.01 ≤ x ≤ 0.33, and for crystals with $x = 10^{-4}$ (dashed line) and $x = 10^{-6}$ (dash-dotted line). For the NH_3 containing liquids, the relaxation times from dielectric spectroscopy (DS) are shown as half-filled symbols. Filled symbols represent NMR correlation times from T_1, F_2, and diffusion measurements. For comparison, we included data on neat water (open circles, ref 39; crosses, ref 40) and on nominally pure ice (stroked symbols: squares, ref 52; diamonds, ref 54; circles, ref 53; triangles, ref 55; stars, this work).

They are in full agreement with the time scales from dielectric and stimulated-echo spectroscopy. The width parameter γ from NMR agrees with the corresponding parameter γ_ε from dielectric spectroscopy.

Finally, the translational dynamics was monitored via Hahn-echo and stimulated-echo techniques employing the proton as nuclear probe. The experiments were carried out in a static magnetic field gradient $g = \partial B/\partial z = (19.3 \pm 1)$ T/m. In Figure 3b we present a set of stimulated proton echo curves for x = 0.26. In order to evaluate the translational self-diffusion coefficient D_t from these data they were fitted using[34]

$$S_2 \propto \exp\left[-D_t\gamma_H^2 g^2 t_p^2\left(t_m + \frac{2}{3}t_p\right)\right]. \tag{5}$$

Here γ_H denotes the gyromagnetic ratio of the proton. The diffusion coefficients resulting from fits to the data such as shown in Figure 3b were transformed to the corresponding time scales $\tau_D = (2/9)R_H^2/D_t$, which assumes validity of the Stokes–Debye equation.[35] The requirement that these time scales should agree with the previously determined ones allows one to estimate the effective hydrodynamic radius R_H of the species performing *rotational* motion. Using R_H = 1.76 Å, we thus obtain the time scales included in Figure 5 as well. For comparison we note that the calculated hydrodynamic radius[36] (or van der Waals radius) of the H_3O^+ ion is 1.88 Å, and for NH_3 it is 1.76 Å.

Using the viscosities η reported in ref 23 in conjunction with our diffusion constants, we estimated the corresponding effective hydrodynamic radius R_H of the *translationally* diffusing moieties in the temperature range 200 K < T < 260 K. By employing the Stokes–Einstein relationship, we obtain $R_H = k_BT/(6\pi\eta D_t) \approx 0.8$ Å. In agreement with the general expectation for diffusion measurements,[35] this small radius suggests that the smallest moieties in our samples, i.e., OH^- species with a hydrodynamic radius of about 1.1 Å[37] and/or protons (via a Grotthus-type of mechanism)[38] dominate the translational diffusion measurements. The detailed assignment should be checked by using oxygen or nitrogen as probe nuclei in diffusion experiments.

IV. DISCUSSION

A. Relaxation Times and Comparison with Aqueous Systems. The correlation times τ resulting from the fits to all presently measured supercooled liquids are summarized in Figure 5. One recognizes that τ is completely insensitive to the ammonia concentration in the range 0.01 ≤ x < 0.33. For comparison, Figure 5 includes dielectric relaxation times of pure water[39,40] that line up smoothly with our results on the ammonia hydrate liquids. The relaxation times shown in Figure 5 are indicative for a super-Arrhenius behavior and were fitted using the Vogel–Fulcher law

$$\tau = \tau_0 \exp\left(\frac{C}{T - T_0}\right). \tag{6}$$

Here, τ_0 is a pre-exponential factor, C a phenomenological constant, and T_0 the temperature at which the extrapolated time constants would diverge. The solid line in Figure 5 (obtained from a fit to the data with x > 0.01) yielded $\tau_0 = 1.3 \times 10^{-15}$ s, C = 1950 K, and T_0 = 71 K. Alternatively, it is common to characterize super-Arrhenius behavior by the fragility index[41] $m = \mathrm{d}\log_{10}(\tau/\mathrm{s})/\mathrm{d}(T_g/T)|_{T=T_g}$ which here gives

dx.doi.org/10.1021/jp407581q | J. Phys. Chem. B 2013, 117, 12157–12163

$m \approx 41$. Although the data of liquid water were not included into our fitting, it is remarkable that this fragility index is very close to the one determined for water from a wealth of aqueous solution data[42] or via different extrapolation procedures.[43] However, some supercooled hydrates show much larger fragility indices ($m \approx 60$ for N_2H_4 and H_2O_2 hydrates[44,45] and m of the order of 100 for sulfuric acid and nitric acid hydrates[46]).

From the parameters entering into eq 6 one can also calculate a glass transition temperature, $T_{g,\alpha} = T(\tau = 100\ s)$, which for the ammonia hydrates turns out to be 121 K. This temperature is significantly lower than the temperature $T_{g,\alpha}$ = 136 K estimated from studies of various aqueous solutions[42] and even from those involving N_2H_4 or H_2O_2 which show a concentration independent T_g.[44,45] Furthermore, 136 K is also the temperature usually quoted for the glass transition of low-density amorphous ice (LDA).[47] However, recent dielectric and calorimetric experiments on specially annealed LDA show[48] that the 100 s time scale conventionally associated with a glass transition is close to 125 K, a temperature compatible with other calorimetric measurements.[49]

It is not clear whether the T_g for our supercooled ammonia solutions ($T_{g,\alpha}$ = 121 K) should be compared with the results of this low-density variant of H_2O ($T_{g,\alpha}$ = 125 K) or, due to the partially ionic character of the constituents in our ammonia solutions, a more compact structure should be expected.[50] It is worthwhile to note that the glass transition of high-density amorphous ice has recently been determined to be about 110 K.[48]

For mole fractions x below 0.01, the samples crystallized already much above temperatures of 200 K. As Figure 5 indicates, at a nominal mole fraction $x \approx 10^{-6}$ the dielectric time constants are practically indistinguishable from those of neat polycrystalline ice. By increasing the level of ammonia doping to $x \approx 10^{-4}$, the dynamics of the crystal becomes much faster, a behavior that is generally expected for ice upon doping.[62]

B. Relaxation Strengths. One of the most remarkable findings of the present work is that the relaxation strength in the $(H_2O)_{1-x}(NH_3)_x$ samples increases almost linearly with x in the studied composition range. This is surprising because the dipole moment of H_2O, μ_{H2O} = 1.85 D,[51] is somewhat larger than that of NH_3, μ_{NH3} = 1.47 D,[51] so one may have guessed initially that the overall relaxation strength decreases slightly with increasing x. The experimentally found linear increase, see Figure 2, thus suggests that $\Delta\varepsilon$ is essentially built up from the electrical dipole moments of the ammonia containing moieties. According to Kargel et al., "free ammonia molecules do not exist; instead the smallest ammonia unit in the liquid is $2H_2O \cdot NH_3$."[23] Hence, the question arises why the dielectric experiment is insensitive to the water molecules that are *not* part of the dihydrate species. In other words, why does the significant fraction of free H_2O molecules, that is present for $x < 0.33$, not show up in the dielectric response? If the free molecules, i.e., those which are not directly part of ammonia involving species, would reorient in a liquid-like fashion, then they are expected to contribute to $\Delta\varepsilon$. Therefore, we are led to suggest that the water molecules might be in a solid-like environment. The straightforward application of this conjecture, however, leads to inconsistencies as well: If NH_3-free ice crystals would be present in a NH_3–H_2O liquid, thus constituting a kind of a slurry, which indeed is envisioned to play a role for cryovolcanic lavas,[23] then these should nevertheless be identifiable from their dielectric signature. However, contributions from NH_3-free ice are not discernible in our experiments as a direct comparison with the dielectric time scales of nominally pure ice crystals shows. In Figure 5 we summarize dielectric relaxation times from various sources.[52−55] This compilation reveals that the dielectric response of *pure* ice crystals, if present, would readily be resolved by the current experiments.

Let us therefore turn to ammonia-doped ice crystals that can be produced for mole fractions up to about x = 0.01.[56,57] Preliminary measurements have shown that such crystals can display significantly shorter relaxation times than pure hexagonal ice and that their relaxation strength can be very small. In a series of measurements,[58] we found a more or less continuous NH_3 doping-induced reduction of the relaxation strength, which becomes as small as $\Delta\varepsilon \approx 10^{-2}$ for $x = 10^{-4}$. The temperature-dependent relaxation time for this sample is provided in Figure 5. The trend obvious from such a sample is indeed expected from Jaccard theory:[59−62] In brief, this theory predicts that doping leads to a decrease of the dielectric relaxation strength[63] as well as of the relaxation time.[64]

Thus, if one assumes that the ammonia containing liquid coexists with NH_3-doped ice crystals that display a strongly suppressed dielectric relaxation strength, one is able to rationalize the linear $\Delta\varepsilon(x)$ dependence seen in Figure 2. Coexistence means that the sample is thought to be decomposed into dielectrically essentially invisible, NH_3 saturated ice crystals and a ammonia dihydrate liquid, which is held responsible for the observed dielectric strength. Such a coexistence is expected to show up in the two-phase solid/liquid region of the ammonia–water phase diagram. Below the peritectic temperature of about 180 K, this solid/liquid mixture should therefore be composed of NH_3 saturated ice crystals and solidified ammonia dihydrate if the conditions of thermodynamic equilibrium apply. In the present situation, the ammonia dihydrate existing near the deep eutectic is severely undercooled so that an increasingly more viscous slurry can be expected to be stable not only near 176 K (ref 65) but also much *below* this temperature. In order to demonstrate a partial crystallization more quantitatively, one should carefully monitor the calorimetric signature of these materials close to their melting points. It is clear that the experimental observation of an almost complete suppression of the dielectric strength of water with a small amount of ammonia added deserves further investigation.

V. CONCLUDING REMARKS

To summarize, our dielectric and NMR results demonstrate that for NH_3 mole fractions $x > 0.01$ the relaxation times of water smoothly overlap with those characterizing the viscous state of the ammonia hydrates. The time scales of the supercooled liquid hydrates turned out to be composition insensitive. On the low-temperature end, a glass transition is obtained where the corresponding T_g closely matches that of the low-density variant of amorphous ice. The fragility index of the ammonia hydrates is about 40 and thus close to the values determined for ultraviscous water from some solution studies, presumably a coincidence. In particular, the fragility indices determined at the glass transition temperatures of the low- and high-density amorphous ices are ≤25 and thus significantly smaller than the values obtained from solution studies.

One of the most puzzling findings of the present work is that the dielectric relaxation strength $\Delta\varepsilon(x)$ of the ammonia

hydrates scales approximately linearly with the ammonia content, despite the quite comparable electrical dipole moments of H_2O and NH_3. This observation can be rationalized by assuming that the samples decompose into dielectrically silent ammonia saturated ice crystals and a liquid phase composed of ammonia dihydrate species that carry the electrical dipole moment. The vanishing dielectric strength was made plausible with reference to preliminary measurements that were found compatible with the theory of Jaccard. More investigations are needed to resolve this issue unambiguously.

AUTHOR INFORMATION

Corresponding Author

*E-mail: roland.bohmer@tu-dortmund.de. Tel: +49-231-755-3514. Fax: +49-231-755-3516.

Notes

The authors declare no competing financial interest.

ACKNOWLEDGMENTS

We thank Agnes Raidt for carrying out a series of dielectric measurements on NH_3-doped ice crystals and Thomas Loerting for stimulating discussion.

REFERENCES

(1) Shin, K.; Kumar, R.; Udachin, K. A.; Alavi, S.; Ripmeester, J. A. Ammonia Clathrate Hydrates as New Solid Phases for Titan, Enceladus, and Other Planetary Systems. *Proc. Natl. Acad. Sci. U.S.A.* **2012**, *109*, 14785−14790.

(2) Chan, J. P.; Giauque, W. F. The Entropy of $NH_3{\cdot}2H_2O$. Heat Capacity from 15 to 300 K. *J. Phys. Chem.* **1964**, *68*, 3053−3057.

(3) Lorenz, R. D.; Shandera, S. E. Physical Properties of Ammonia-Rich Ice: Application to Titan. *Geophys. Res. Lett.* **2001**, *28*, 215−218.

(4) Fortes, A. D.; Wood, I. G.; Brodholt, J. P.; Alfredsson, M.; Vočadlo, L.; McGrady, G. S.; Knight, K. S. A High-Resolution Neutron Powder Diffraction Study of Ammonia Dihydrate $ND_3{\cdot}2D_2O$. Phase I. *J. Chem. Phys.* **2003**, *119*, 10806−10813.

(5) Fortes, A. D.; Wood, I. G.; Brodholt, J. P.; Vočadlo, L. Structure, Ordering and Equation of State of Ammonia Dihydrate ($NH_3{\cdot}2H_2O$). *Icarus* **2003**, *162*, 59−73.

(6) Bertie, J. E.; Shehata, M. R. Ammonia Dihydrate: Preparation, X-Ray Powder Diffraction Pattern and Infrared Spectrum of $NH_3{\cdot}2H_2O$ at 100 K. *J. Chem. Phys.* **1984**, *81*, 27−29.

(7) Lebrun, N.; Mahe, F.; Foulon, M.; Gors, C.; Petit, J. C. Thermal Behaviour of Nitric Acid Dihydrate in 1:2 HNO_3/H_2O Solutions. *Can. J. Phys.* **2003**, *81*, 61−69.

(8) Moore, M. H.; Ferrante, R. F.; Hudson, R. L.; Stone, J. N. Ammonia−Water Ice Laboratory Studies Relevant to Outer Solar System Surfaces. *Icarus* **2007**, *190*, 260−273.

(9) Lorenz, R. D. Preliminary Measurements of the Cryogenic Dielectric Properties of Water−Ammonia Ices: Implications for Radar Observations of Icy Satellites. *Icarus* **1998**, *136*, 344−348.

(10) Gross, G. W. Nitrates in Ice: Uptake; Dielectric Response by the Layered Capacitor Method. *Can. J. Phys.* **2003**, *81*, 439−450.

(11) Rollet, A.-P.; Vuillard, G. Contribution a l'Etude de l'Etat Vitreux et de la Cristallisation des Solutions Aqueuses. *C. R. Acad. Sci.* **1956**, *243*, 383−386.

(12) Yarger, J.; Lunine, J. L.; Burke, M. Calorimetric Studies of the Ammonia−Water System with Application to the Outer Solar System. *J. Geophys. Res.* **1993**, *98*, 13109−13117.

(13) Leliwa-Kopystynski, J.; Maruyama, M.; Nakajima, T. The Water−Ammonia Phase Diagram up to 300 MPa: Application to Icy Satellites. *Icarus* **2002**, *159*, 518−528.

(14) Fortes, A. D.; Grindrod, P. M.; Trickett, S. K.; Vočadlo, L. Ammonium Sulfate on Titan: Possible Origin and Role in Cryovolcanism. *Icarus* **2007**, *188*, 139−153.

(15) Grindrod, P. M.; Fortes, A. D.; Nimmo, F.; Feltham, D. L.; Brodholt, J. P.; Vočadlo, L. The Long-Term Stability of an Aqueous Ammonium Aulfate Ocean Inside Titan. *Icarus* **2007**, *197*, 137−151.

(16) Fortes, A. D.; Wood, I. G.; Vočadlo, L.; Knight, K. S.; Marshall, W. G.; Tucker, M. G.; Fernandez-Alonso, F. Phase Behaviour and Thermoelastic Properties of Perdeuterated Ammonia Hydrate and Ice Polymorphs from 0 to 2 GPa. *J. Appl. Crystallogr.* **2009**, *42*, 846−866.

(17) Loveday, J. S.; Nelmes, R. J. The Ammonia Hydrates: Model Mixed-Hydrogen-Bonded Systems. *High Pressure Res.* **2004**, *24*, 45−55.

(18) McKinnon, W. B. Sublime Solar System Ices. *Nature* **1995**, *375*, 535−536.

(19) Mitri, G.; Showman, A. P.; Lunine, J. I.; Lopes, R. M. C. Resurfacing of Titan by Ammonia−Water Cryomagma. *Icarus* **2008**, *196*, 216−224.

(20) Kargel, J. S. Ammonia−Water Volcanism on Icy Satellites: Phase Relations at 1 atm. *Icarus* **1992**, *100*, 556−574.

(21) Vuillard, G. Les Diagrammes de Transformation Verre ↔ Liquide. *Publ. Sci. Univ. Alger. B* **1957**, *3*, 80−101.

(22) van Kasteren, P. H. G. The Crystallization Behaviour and Caloric Properties of Water/Ammonia Mixtures between 70 and 300K. *Bull. Inst. Froid. Annexe* **1973**, *4*, 81−87.

(23) Kargel, J. S.; Croft, S. K.; Lunine, J. I.; Lewis, I. S. Rheological Properties of Ammonia−Water Liquids and Crystal-Liquid Slurries: Planetological Applications. *Icarus* **1991**, *89*, 93−112.

(24) The molar amount n_{H_2O} to be added to the aqueous solution ($n_{NH_3(sol)} \approx 26.07$; $n_{H_2O(sol)} \approx 73.93$) for the intended molar concentration x is given by $n_{H_2O} = n_{NH_3(sol)}/x - 100$. Then, we obtained the appropriate volume ratio $V_{NH_3(sol)}:V_{H_2O}$ from $(n_{NH_3(sol)}M_{NH_3} + n_{H_2O(sol)}M_{H_2O})/\rho_{sol}:(n_{H_2O}M_{H_2O})/\rho_{H_2O}$. M denotes the molar mass, and the density of the solution is $\rho_{sol} = 0.903$ g/mol.

(25) Schmidt-Rohr, K.; Spiess. H. W. *Multidimensional Solid-State NMR and Polymers*; Academic Press: London, U.K., 1994.

(26) Wagner, H.; Richert, R. Equilibrium and Non-Equilibrium Type β-Relaxations: D-Sorbitol versus *o*-Terphenyl. *J. Phys. Chem. B* **1999**, *103*, 4071−4077.

(27) Davidson, D. W.; Cole, R. H. Dielectric Relaxation in Glycerol, Propylene Glycol, and *n*-Propanol. *J. Chem. Phys.* **1951**, *19*, 1484−1490.

(28) See, e.g., Fanfoni, M.; Tomellini, M. The Johnson−Mehl−Avrami−Kolmogorov Model: A Brief Review. *Il Nuovo Cimento D* **1998**, *20*, 1171−1182. Weinberg, M. C. A Few Topics Concerning Nucleation and Crystallization in Glasses. *J. Non-Cryst. Solids* **1999**, *255*, 1−14 and references cited therein.

(29) For a more detailed discussion, see Sharples , A. *Introduction to Polymer Crystallization*; Edward Arnold Publisher Ltd.: London, U.K., **1966.**,

(30) Rabideau, S. W.; Waldstein, P. Deuteron Magnetic Resonance of Polycrystalline Deuteroammonia. *J. Chem. Phys.* **1966**, *45*, 4600−4603.

(31) Laaksonen, A.; Wasylishen, R. E. Calculations of ^{14}N and ^{2}H Nuclear Quadrupolar Coupling Constants for Liquid Ammonia. *Z. Naturforsch. A* **1995**, *50a*, 137−144.

(32) Böhmer, R.; Diezemann, G.; Hinze, G.; Rössler, E. Dynamics of Supercooled Liquids and Glassy Solids. *Prog. Nucl. Magn. Reson. Spectrosc.* **2001**, *39*, 191−267.

(33) Bloembergen, N.; Purcell, E. M.; Pound, R. V. Relaxation Effects in Nuclear Magnetic Resonance Absorption. *Phys. Rev.* **1948**, *73*, 679−712.

(34) Geil, B. Measurement of Translational Molecular Diffusion Using Ultrahigh Magnetic Field Gradient NMR. *Concepts Magn. Reson.* **1998**, *10*, 299−321.

(35) Chang, I.; Sillescu, H. Heterogeneity at the Glass Transition: Translational and Rotational Self-Diffusion. *J. Phys. Chem. B* **1997**, *101*, 8794−8801.

(36) Edward, J. T. Molecular Volumes and the Stokes−Einstein Equation. *J. Chem. Educ.* **1970**, *47*, 261−270.

(37) Marcus, Y. Volumes of Aqueous Hydrogen and Hydroxide Ions at 0 to 200° C. *J. Chem. Phys.* **2012**, *137*, 154501.

(38) Marx, D. Proton Transfer 200 Years after von Grotthus: Insights from ab Initio Simulations. *ChemPhysChem* **2006**, *7*, 1848−1870.
(39) Rønne, C.; Keiding, S. R. Low-Frequency Spectroscopy of Liquid Water Using THz-Time Domain Spectroscopy. *J. Mol. Liq.* **2002**, *101*, 199−218.
(40) Buchner, R.; Barthel, J.; Stauber, J. The Dielectric Relaxation of Water Between 0 and 35 °C. *Chem. Phys. Lett.* **1999**, *306*, 57−63.
(41) Böhmer, R.; Ngai, K. L.; Angell, C. A.; Plazek, D. J. Nonexponential Relaxations in Strong and Fragile Glass Formers. *J. Chem. Phys.* **1993**, *99*, 4201−4209.
(42) Capaccioli, S.; Ngai, K. L. Resolving the Controversy on the Glass Transition Temperature of Water? *J. Chem. Phys.* **2011**, *135*, 104504/1−12.
(43) Schmidtke, B.; Petzold, N.; Kahlau, R.; Hofmann, M.; Rössler, E. A. From Boiling Point to Glass Transition Temperature: Transport Coefficients in Molecular Liquids Follow Three-Parameter Scaling. *Phys. Rev. E* **2012**, *86*, 041507/1−6.
(44) Minoguchi, A.; Richert, R.; Angell, C. A. Dielectric Relaxation in Aqueous Solutions of Hydrazine and Hydrogen Peroxide: Water Structure Implications. *J. Phys. Chem. B* **2004**, *108*, 19825−19830.
(45) Minoguchi, A.; Richert, R.; Angell, C. A. Dielectric Studies Deny Existence of Ultraviscous Fragile Water. *Phys. Rev. Lett.* **2004**, *93*, 215703/1−4.
(46) Frey, M.; Didzoleit, H.; Gainaru, C.; Böhmer, R. Dynamics in Glass Forming Sulfuric and Nitric Acid Hydrates. *J. Phys. Chem. B* **2013**, DOI: 10.1021/jp407588j.
(47) Angell, C. A. Insights into Phases of Liquid Water from Study of Its Unusual Glass-Forming Properties. *Science* **2008**, *319*, 582−587.
(48) Amann-Winkel, K.; Gainaru, C.; Handle, P. H.; Seidl, M.; Nelson, H.; Böhmer, R.; Loerting, T. Water's Second Glass Transition, *Proc. Natl. Acad. Sci.* (accepted for publication).
(49) Handa, Y. P.; Mishima, O.; Whalley, E. High-Density Amorphous Ice. III. Thermal Properties. *J. Chem. Phys.* **1986**, *84*, 2766−2770.
(50) This conjecture is corroborated by the finding of partial molar volumes for ammonia in dilute aqueous solutions, see Kaulgud, M. V.; Pokale, W. K. Temperature of Maximum Density Behaviour of Ammonia in Water. *J. Chem. Soc., Faraday Trans.* **1992**, *88*, 997−1001.
(51) Nelson. Jr., R. D.; Lide, Jr., D. R.; Maryott, A. A. *Selected Values of Electric Dipole Moments for Molecules in the Gas Phase*, National Standard Reference Data Series, National Bureau of Standards 10; NIST: Gaithersburg, MD, 1967.
(52) Kawada, S. Dielectric Anisotropy in Ice I_h. *J. Phys. Soc. Jpn.* **1978**, *44*, 1881−1886.
(53) Johari, G.; Whalley, E. The Dielectric Properties of Ice I_h in the Range 272−133 K. *J. Chem. Phys.* **1981**, *75*, 1330−1340.
(54) Tyagi, M.; Murthy, S. S. N. Dielectric Relaxation in Ice and Ice Clathrates and Its Connection to the Low-Temperature Phase Transition Induced by Alkali Hydroxides as Dopants. *J. Phys. Chem. A* **2002**, *106*, 5072−5080.
(55) Gough, S. R.; Davidson, D. W. Dielectric Behavior of Cubic and Hexagonal Ices at Low Temperatures. *J. Chem. Phys.* **1970**, *52*, 5442−5449.
(56) Hubmann, M. Effect of Pressure on the Dielectric Properties of Ice I_h Single Crystals Doped with NH_3 and HF. *J. Glaciology* **1978**, *21*, 161−172.
(57) Arias, D.; Levi, L.; Lubart, L. Electrical Properties of Ice Doped with NH_3. *Trans. Faraday Soc.* **1966**, *62*, 1955−1962.
(58) In another series of experiments, the observations described in the main text could not be fully reproduced.
(59) Jaccard, C. Theoretical and Experimental Studies of the Electrical Properties of Ice. *Helv. Phys. Acta* **1959**, *32*, 89−128.
(60) Jaccard, C. Thermodynamics of Irreversible Processes Applied to Ice. *Phys. Kondens. Mater.* **1964**, *3*, 99−118.
(61) Nagle, J. F. Theory of the Dielectric Constant of Ice. *Chem. Phys.* **1979**, *43*, 317−328.
(62) Petrenko, V. F.; Whitworth, R. W. *Physics of Ice*; Oxford University Press: Oxford, U.K., 1999.
(63) This result is also shown by the data in ref 57, which extend down to T = 233 K.
(64) For doped ices, the Jaccard theory predicts that the relaxation time associated with a defect of type i (as, e.g., induced by NH_3 doping) should be given by $\tau_i \propto e_i/(n_i\mu_i k_B T) \propto \Delta\varepsilon_i$. Here e_i, n_i, and μ_i are effective charge, number density, and mobility, respectively, of this defect type, and $\Delta\varepsilon_i$ is its contribution to the relaxation strength. Within this theory, an (approximate) proportionality between τ_i and $\Delta\varepsilon_i$ arises because each transport step of a defect in the ice crystal is accompanied by a reorientation of a water molecule. Starting from a hypothetical defect-free crystal that is electrically fully polarized (of course according to Curie's law at a given temperature), introduction of a defect does enable defect motion; hence, it decreases τ_i. In addition, the motion of defects also rotates dipole moments away from orientations corresponding to maximum possible polarization; hence, it reduces $\Delta\varepsilon$.
(65) In refs 18 and 23, photos of such slurries are published from which a whitish, opaque appearance of the ammonia−water mixtures is obvious. We interpret this as a strong hint for the two-phase nature of these samples.